Annealing and Ultraviolet Treatment of Plasma Fluorocarbon Films for Enhanced Cohesion and Stability

P. Chevallier,[1] S. Holvoet,[1] S. Turgeon,[1] P. Horny,[1] J. J. Pireaux,[2] D. Mantovani[1]

[1]*Laboratory for Biomaterials and Bioengineering, Department of Materials Engineering and University Hospital Research Center, Laval University, Quebec City, Quebec G1K 7P4, Canada*
[2]*Laboratoire Interdisciplinaire de Spectroscopie Electronique, Facultés Universitaires Notre-Dame de la Paix (FUNDP), University of Namur, 61 Rue de Bruxelles, B-5000 Namur, Belgium*

Received 16 December 2009; accepted 14 March 2010
DOI 10.1002/app.32621
Published online 9 July 2010 in Wiley InterScience (www.interscience.wiley.com).

ABSTRACT: Stents, commonly used for the treatment of cardiovascular diseases, are mainly made of 316L stainless steel. They are, however, prone to corrosion when they are in contact with human body fluid. To prevent this corrosion process and to ameliorate their patencies, in this study, we used a strategy to cover stent materials with a protective fluorocarbon layer deposited by plasma polymerization. In an approach to optimize its cohesion properties and stability, posttreatments, namely, thermal annealing and UV irradiation, were applied on the ultrathin fluorocarbon film. A combination of X-ray photoelectron spectroscopy, polarized near-edge X-ray absorption fine-structure spectroscopy, and time-of-flight secondary ion mass spectrometry demonstrated that UV treatment led to chain scission and film crosslinking and, in this way, decreased the amount and/or size of nanoscaled defects originally present in the films. Annealing on the other hand induced a film reorganization in favor of longer, well-ordered fluorocarbon chains. However, a deformation process that was applied to study the film adhesion properties induced chain scissions with reorganization. Aging tests exhibited an oxidation of the topmost layer for both the as-deposited and posttreated samples. Finally, the film stability was improved after UV treatment for both the nondeformed and deformed samples. © 2010 Wiley Periodicals, Inc. J Appl Polym Sci 118: 3176–3186, 2010

Key words: annealing; fluoropolymers; plasma polymerization

INTRODUCTION

Depositions of thin films onto substrates have been profusely investigated because this technique permits one to improve the surface properties without altering the material itself. Several approaches can be used, such as dip, spin, or spray coating; chemical vapor deposition; and plasma polymerization. However, whatever the application, the coating should have adequate properties, such as good adhesion on the material and stability in the long term. In the case of an organic coating deposited onto a metallic substrate, the adhesion is often a problem because of the low interactions between the polymeric layer and the substrate. Indeed, films deposited by dip, spin, and spray coating and chemical vapor deposition have exhibited a lack of adhesion when submitted to deformation, friction, or shear stress. Delamination and/or cracks in the films were observed.[1] However, the plasma polymerization process permitted better adhesion between the polymeric layer and the substrate because of the initial activation of the surface. Moreover, this technique can be used to rapidly deposit thin polymer films onto a wide variety of substrates, such as polymers,[2–6] stainless steels,[7] other metals,[8,9] glass,[4] and silicon.[8,10] Furthermore, depending on the gas used during this process, different properties can be assessed, such those of as hydrophilic or hydrophobic surfaces, nonfouling or protective layers, or functionalization of an inert surface.[2,7] For example, it has been previously shown that metals can be effectively protected against corrosion by the deposition of thin plasma polymer coatings.[8,11–14]

With all these parameters considered and to produce a thin film on stents as a protective layer from corrosion induced by the physiological environment, thin-film deposition by plasma polymerization appeared to be the best approach. Placed inside partially blocked arteries to prevent the obstruction of blood flow and to act as internal scaffolding,[15] stents are thin metal wire mesh tubes mainly made of 316L

Correspondence to: D. Mantovani Laboratory for Biomaterials and Bioengineering, Department of Mining, Metallurgy and Materials Engineering, Pavillon Adrien-Pouliot, 1745-E, Laval University, Quebec City, Quebec G1K 7P4, Canada (diego.mantovani@gmn.ulaval.ca).

Contract grant sponsors: Natural Sciences and Engineering Research Council of Canada, University Hospital Research Center (St. François d'Assise Hospital), Quebec City.

© 2010 Wiley Periodicals, Inc.

stainless steel. During the implantation procedure, they are submitted to a plastic deformation of up to 25%.[16] Their corrosion, which leads to ion release in the physiological environment, represents a potential source for further complications at the clinical level.[17] In fact, possible corrosion products include chromium and nickel, two elements classified as carcinogenic by the International Agency for Research on Cancer.[18] To evaluate the efficiency of a coating on stents, the adhesion, barrier effectiveness, durability, and stability of the coating should be demonstrated, as required by the U.S. Food and Drug Administration.[19–21]

In this context, to improve the long-term performance and safety of stainless steel stents, a Teflonlike film was chosen, as Teflon has already been used for cardiovascular grafts for decades. Indeed, Teflon is chemically inert and nondegradable when submitted to the shear stress induced by blood flow and does not induce a severe immune response. Therefore, a multistep process was previously developed in our laboratory to isolate the stainless steel surface from the body fluid by the deposition of an ultrathin ($\sim$ 35 nm) uniform and cohesive plasma-polymerized fluorocarbon (Teflonlike) coating.[22] X-ray photoelectron spectroscopy (XPS) analyses showed a continuous coating that resisted plastic deformations up to 25%.[22] Recent time-of-flight secondary ion mass spectrometry (ToF–SIMS) and near-edge X-ray absorption fine structure spectroscopy (NEXAFS) data, however, indicated the presence of a certain density of pores or nanopinholes in the films.[23] These nanodefects could compromise the cohesion and stability of the fluorocarbon coatings and, in this way, hamper the long-term patency of these medical devices. Indeed, aging tests in aqueous media have demonstrated oxidation and reorganization of the film, mainly due to water infiltration through nanopinholes.[24]

In an attempt to reduce the density of film defects and, therefore, prevent water infiltration through the films, posttreatments were investigated. These treatments should lead to a more crosslinked polymeric film coating by the induction of chain reorganization, without alteration of the polymer/metal interface. Crosslinking in polymer science can be obtained in different ways, such as annealing, γ radiation, UV irradiation, X-rays, ions, electrons beams, and plasmas.[25] Plasma activation would appear practical, but it acts only on the topmost layers ($\sim$ 10 Å).[26,27] To modify the entire film thickness ($\sim$ 35 nm) and to retain its mechanical behavior (the ability to follow the 25% plastic deformation), UV radiation and thermal annealing are preferred.

The temperature of annealing should be high enough to permit reorganization of the polymeric layer, which depends on the initial film composition and its crystallinity: for example, the upper temperatures of usage range for polytetrafluoroethylene (PTFE; CF_2—CF_2) between 180 and 260°C, for poly (vinylidene fluoride) (CH_2—CF_2) between 135 and 150°C, and for poly(vinyl fluoride) (CH_2—CHF) between 150 and 200°C.[28] In our case, as the fluorocarbon film deposited by plasma polymerization process had a not-so-well-defined chemical structure, the temperature effects on the film composition were screened between 125 and 250°C.

For UV irradiation, the selection of the wavelength is important for breaking target chemical bonds. Aliphatic C—F bonds are known to be cleaved by UV light with wavelengths around 240 nm, whereas C—C and C—H bond scission in fluorinated polymers occurs between 260 and 280 nm, depending on the chemical environment.[29] In this study, UV irradiation was chosen at 254 nm, as this wavelength provided enough energy to induce C—C and C—H scissions in the fluorocarbon films without damaging the CF_2 bonds. Thereafter, the effect of UV irradiation at 254 nm was screened at different durations of a constant UV density.

In this study, the influence of these posttreatments, thermal annealing, and UV irradiation on the chemical composition, morphology, and stability of the films was investigated with XPS, polarized NEXAFS, and ToF–SIMS.

EXPERIMENTAL

Materials

Disks 12.7 mm in diameter and 0.5 mm thick were punched from 316L stainless steel plates (Goodfellow, Devon, PA) with the following compositions (wt %): Cr, 16.00–18.00; Ni, 10.00–14.00; Mo, 2.00–3.00; Mn, $\leq$2.00; Si, $\leq$1.00; C, $\leq$0.08; P, $\leq$0.045; S, $\leq$0.03; and Fe, balance. Before plasma polymerization, the disks were subjected to a pretreatment described in detail elsewhere and consisting essentially of four steps:[30] (1) ultrasonic cleaning, (2) electropolishing, (3) acidic dipping, and (4) pulsed-H_2 (Bocgaz, Quebec, Canada, 99.999% purity) plasma etching. The plasma deposition was performed at 11 cm below the glow region.[22] The feed gases used during plasma polymerization were a mixture of 94% C_2F_6 (Sigma-Aldrich, 98+ % purity) and 6% H_2. The pulsed plasma deposition was realized with the following parameters: Radio frequency (RF) peak power input = 150 W (13.56 MHz), t_{on} (on time) = 5 ms, t_{off} (off time) = 90 ms, gas pressure = 0.93 mbar, total gas flow rate = 20 sccm, and duration = 5 min.

Deformation method

The coated samples were plastically deformed up to 25% with a custom-made small-punch test device mounted on a SATEC T20000 testing machine (Instron,

Norwood, MA), as previously described.[22] All deformations were performed at room temperature at a displacement rate of 0.05 mm/s and a load of 2200 N. All subsequent analyses were performed on the topmost part of the deformed samples, where the 25% deformation had occurred.

Posttreatments

We performed thermal annealing by heating the specimens at a constant temperature (between 125 and 250°C) for 2 h in a vacuum desiccator. After annealing, the temperature was allowed to equilibrate to room temperature. UV treatment was realized by irradiation of the samples at a 254-nm wavelength with a mercury lamp (Philips UVc-Hg, TUV 30W/G30T8, Eindhoven, The Nederlands) at a constant power density of 3.5 W/cm^2 under atmospheric conditions. All samples were stored *in vacuo* before analysis.

Surface aging

Aging tests were carried out in deionized water for 2 weeks in an incubator at 37 ± 2°C. Each sample was placed in a high-density polyethylene sample holder to expose only its coated surface to the buffer (0.64 and 0.20 cm^2 for the flat and deformed samples, respectively). Before the aging tests, the sample holders and aging medium were sterilized by an autoclave to prevent bacterial propagation during aging. Samples were manipulated with sterilized (70% ethanol) tweezers under a laminar flow hood. After aging, samples were removed from their holders, thoroughly rinsed with deionized water, and finally wiped with medical-grade compressed air.

Characterization of the ultrathin coating

The surface chemical composition was analyzed by XPS. Three samples per treatment were analyzed, and three different spots were examined on each sample. These analyses were performed with an X-ray photoelectron spectrometer (XPS-PHI 5600-ci spectrometer, Physical Electronics, Eden Prairie, MN). Charge compensation was not necessary. Survey and high-resolution spectra were acquired with the Kα line of standard aluminum (Kα = 1486.6 eV) and magnesium (Kα = 1253.6 eV) X-ray sources, respectively. Quantification was performed with the O1s, F1s, and C1s peak areas from the survey spectra multiplied by their respective sensitivity factors and then normalized by their total. The curve fitting for the high-resolution C (1s) peaks was determined by means of a least squares peak-fitting procedure with a Shirley-type background. Five spectral components were used, which represented the five major types of chemical environments of a carbon atom in a fluorocarbon structure: C—C/C—H (hydrocarbon), *C*—CF_x, CF, CF_2, and CF_3. All components were assigned with the same full width at half-maximum. Their respective positions were not fixed. With the binding energy (BE) of C—C/C—H assumed to be 285.0 eV, the mean BEs obtained for the different C (1s) components were 286.8 eV (*C*—CF_x), 289.4 eV (CF_x), 292.0 eV (CF_2), and 294.0 eV (CF_3). These values and the corresponding assignments agreed well with data published in the literature.[31]

X-ray photoemission electron microscopy (X-PEEM) were performed at the Canadian light source (CLS) on a soft X-ray spectromicroscopy beamline 10ID-1 with a 75-mm generalized Apple II elliptically polarizing undulator, which provided an intense beam in the 130–2500-eV energy range with a user-specified polarization. An infinity-corrected plane-grating monochromator with a vertical dispersion plane was applied to the beam output with a nominal energy resolution higher than 3000. In a 50-μm spot, the flux was approximately 10^{12} γ/s (0.1% bandwidth (BW) at 100 mA) at 250 eV. The end station included an Elmitec GmbH PEEM system with a spot size of 100 × 100 μm^2. All data were processed with AXIS2000. The NEXAFS spectra were extracted from the X-PEEM images and normalized to the mesh current to account for the absorption along the beamline. The average of three different locations on the surface were used and normalized to 1 to allow comparisons between the samples.

ToF–SIMS analyses were realized with a ToF–SIMS IV (ION-ToF GmbH, Münster, Germany) with a 25-keV Ga^+ analysis gun. The gallium current was 1.6 pA, the beam hit the target at an angle of 45°, and the primary ion dose density was below the static secondary ion mass spectrometry limit of 10^{13} ions/cm^2.[32,33] Ions used for the mass calibration were H+ (m/z = 1), C+ (m/z = 12), and C_2F_5+ (m/z = 119). For spectral acquisition, positive-ion mass spectra were acquired from a 500 × 500 μm^2 area, and mass fragment ratios were directly calculated from the mass intensities. The ToF–SIMS in negative mode is not detailed in this article, as the degradation/defluorination processes, which could be detected by C_xF_y moieties, were very well detected in the positive mode.[34]

Fourier transform infrared (FTIR) spectroscopy was done with a Nicolet Magna 550 FTIR spectrometer (Thermo-Nicolet, Madison, WI) in the attenuated total reflectance (ATR) mode with a Split Pea attachment (Harrick Scientific Corp., Ossining, NY). One hundred fifty scans were recorded with a spectral resolution of 4 cm^{-1}.

Atomic force microscopy studies were performed with the tapping mode of a Dimension 3100 atomic microscope (Veeco, Woodbury, NY) with an etched silicon tip (tip radius <10 nm). The surface

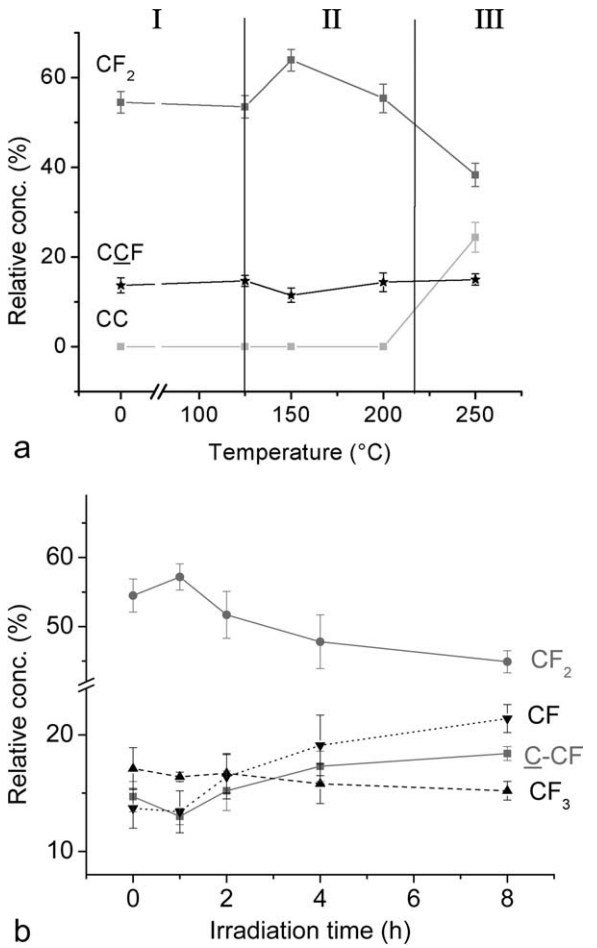

Figure 1 XPS high-resolution data for (a) thermally annealed and (b) UV-irradiated flat specimens.

roughness was calculated and expressed as the root mean square roughness parameter (R_{RMS}) from three areas of 20 × 20 μm^2 per sample. Visualization and analysis of the morphology were done with WSxM software.[35]

The film thickness of the nondeformed samples was measured with a spectroscopic ellipsometer (UVISEL, HORIBA Yvon Jobin, Edison, NJ) with 100 wavelengths from 400 to 800 nm at an incidence angle of 70°.

RESULTS AND DISCUSSION

Optimization of the posttreatment experimental parameters

XPS survey and carbon (1s) high-resolution spectra were acquired to determine the possible effects of the two posttreatments on the F/C ratio and the percentage of different carbon functionalities in the film (C—C, *C*—CF, CF, CF_2, and CF_3), respectively.

The effect of thermal annealing was screened over a temperature range of up to 250°C [Fig. 1(a)]. Although no nonfluorinated carbon moieties (C—C) were measured up to 200°C, the number rose to 25% thereafter at 250°C, and the CF_2 (and *C*—CF) plot displayed a more complex trend. The percentage of the latter functionalities (CF_2, specifically) stayed rather constant up to 125°C (at 55 ± 3%), increased at 150°C (up to 64 ± 2%), and dropped thereafter to its initial value at 200°C. A further increase in the temperature made the latter CF_2 content decrease. This temperature scan could be divided into three regions: a first region (25–125°C) without any significant effect, a second region (125–200°C) featured by a film reorganization, and a third region (>200°C) wherein film degradation (defluorination) started to occur. The thermal stability of the deposited CF_x films was, thus, limited to 200°C, which was slightly lower compared to published data in the literature. In earlier work on CF_x films by Maia da Costa et al.,[36] fluorine concentrations remained essentially constant at annealing temperatures up to 300°C; this was followed by a strong decrease at higher temperatures. In other work by Cruden et al.,[37] slow decomposition (10^{-4} %/h) was observed as low as 230°C, although appreciable weight loss (0.1%/h) was not observed below 440°C. The higher thermal stability of the latter films was probably directly related to their more crosslinked character, as these films contained higher amounts of CF, *C*—CF, and C—C moieties. However, in this study, the coating composition and stability was closer to PTFE and fluorocarbon films (with upper use temperatures between 180 and 250°C and 150–220°C, respectively).[38] In what follows, thermal annealing was performed at 150°C.

The effect of UV irradiation was screened at different durations of constant UV density. Up to 8 h of treatment, no significant film degradation was monitored, as no C—C functionalities were measured by XPS. The percentages of CF_2 started to decrease, whereas the numbers of *C*—CF and CF functionalities increased after 2 h of treatment [Fig. 1(b)]; this demonstrated the crosslinking effect of UV irradiation on the thin fluorocarbon films. Surveys on specimens irradiated for 40 h exhibited the presence of metals (0.3% chromium and associated oxides), which indicated film cracking. From this point on, the duration of UV treatment was set at 2 h to benefit from crosslinking phenomena (which were not significant after 1 h) and to simultaneously prevent excessive film stiffening.

Effect of the posttreatment on the surface chemical composition: A detailed study

Subsequently, specimens were subjected to the posttreatments in the conditions discussed previously and studied with XPS before and after plastic deformation (Table I). None of the survey spectra showed the presence of Cr or Fe in either the nondeformed

TABLE I
F/C and O/C Ratios (Calculated from the XPS Survey Data) and *C*—CF, CF, CF_2, and CF_3 Contents (Obtained from XPS C1s High-Resolution Scans)

	Deformation	F/C	O/C	% *C*—CF	% CF	% CF_2	% CF_3
As-deposited	0%	2.09 ± 0.03	0.01 ± 0.01	14 ± 2	15 ± 1	55 ± 3	17 ± 2
	25%	2.00 ± 0.04	0.01 ± 0.01	15 ± 2	16 ± 1	53 ± 2	16 ± 1
UV-treated	0%	1.90 ± 0.06	0.02 ± 0.01	16 ± 2	15 ± 2	52 ± 3	17 ± 2
	25%	1.64 ± 0.08	0.03 ± 0.01	22 ± 2	22 ± 2	42 ± 2	14 ± 1
Annealed	0%	2.06 ± 0.05	0.01 ± 0.01	11 ± 2	11 ± 1	64 ± 2	14 ± 1
	25%	1.86 ± 0.06	0.03 ± 0.01	16 ± 2	16 ± 2	52 ± 5	16 ± 2

All data are presented as a function of treatment and before and after deformation.

or deformed samples (not shown). The treatments, thus, certainly did not enlarge the amount of exposed surface to a value higher than about 1% (corresponding to the sensitivity of XPS for the latter metals). In addition, neither posttreatment induced degradation of the films, as no adventitious (defluorinated) carbon was detected.

Compared to the as-deposited specimen, the F/C ratio decreased slightly after the UV treatment (from 2.09 ± 0.03 to 1.90 ± 0.06), with no significant increase in O/C (from 0.01 ± 0.01 to 0.02 ± 0.01). Moreover, a minor decrease in the CF_2 content was observed after UV treatment compared to the as-deposited specimens (52 ± 3%), whereas the percentage of *C*—CF increased slightly (to 16 ± 2%). This phenomenon was probably due to crosslinking induced by UV irradiation.

In contrast, after thermal annealing, the F/C ratio remained unchanged compared to the as-deposited films (2.06 ± 0.05). The proportion of CF_2 groups in the film significantly increased from 55 ± 3 to 64 ± 2%, whereas simultaneously, the amount of *C*—CF groups dropped from 14 ± 2 to 11 ± 2%. Thermal annealing apparently induced a rearrangement favoring long polymer chains, which were richer in CF_2. The latter was also observed in recent work by Gnanappa et al.,[39] where annealing at 100°C cracked CF_3 moieties on the surface of 300-nm thin fluorocarbon films and enhanced CF_2 groups, which, thus, created a high number of dangling bonds on the surface. In subsequent stability studies, these authors also reported decreased degradation rates compared to unannealed films.

After deformation, a slight increase in the oxygen content was observed for all of the samples (Table I). The latter was due to the deformation procedure itself (carried out in atmospheric conditions), during which oxygen was incorporated into the top layers of the film. Indeed, ToF–SIMS experiments on the deformed samples proved earlier to be accompanied with polymeric chain scission and radical-based defluorination and oxidation.[23] This was confirmed by the decrease in the CF_2 content and the increase in the 286.8-eV band, which should have been assigned to both the *C*—CF and C—O functionalities (Table I).[40] Indeed, the incorporation of oxygen (an increase in the O/C ratio) during the deformation of posttreated specimens was directly correlated to the variation in the *C*—CF/C—O percentages.

In addition, NEXAFS was applied as a complementary analysis to XPS. The scanned absorption edges included the C K-shell, F K-shell as well as the Fe $L_{2,3}$-shell electronic transitions. NEXAFS analyses were performed with an incident beam polarized at 0 and −90° (with the electric field quasi-perpendicular and parallel to the surface, respectively). Indeed, polarized NEXAFS can yield valuable information on the specific orientation of the polymer chains relative to the surface.[41]

The C (1s) NEXAFS spectra for some posttreated specimens are shown in Figure 2. The major peaks, which were visible in the C (1s) region, were at 285 eV (due to C 1s to π* C=C transitions), 288 eV (due to C 1s to σ* C—H transitions), 290 eV (due to C 1s to π* C=CF_2 transitions), and 295 eV (due to C 1s to σ* C—C transitions). The peaks of CF contributions were present at 293 and 298 eV (due to C 1s to σ* C—F transitions).[42] There was also a broad absorbance band between 289 and 298 eV, which was similar to that described by Castner et al.,[43] which was attributed to randomly orientated polymer chains. The NEXAFS F (1s) and Fe (2p) regions are displayed together in Figure 3 and showed a broad F peak and two Fe peaks ($2p_{1/2}$ and $2p_{3/2}$). The F peak was due to a combination of F 1s to σ* C—F and F 1s to σ* C—C transitions.[44] The Fe signal had a distinct double peak in the $2p_{3/2}$ region assigned to metallic Fe (at 708 eV) and to Fe_2O_3 and Fe_3O_4 (at 709 eV) due to the presence of iron oxides in the interfacial region.[45] Alternatively, the latter 709-eV transition could also be associated with metallic fluorines.[46]

NEXAFS analyses after UV irradiation exhibited an important modification of the polymer composition as compared to the as-deposited films [Fig. 2(a)]. Indeed, the UV treatment led to a significant increase in the signal at 285 eV (C 1s to π* C=C transition) and at 295 eV (C 1s to σ* C—C transition).

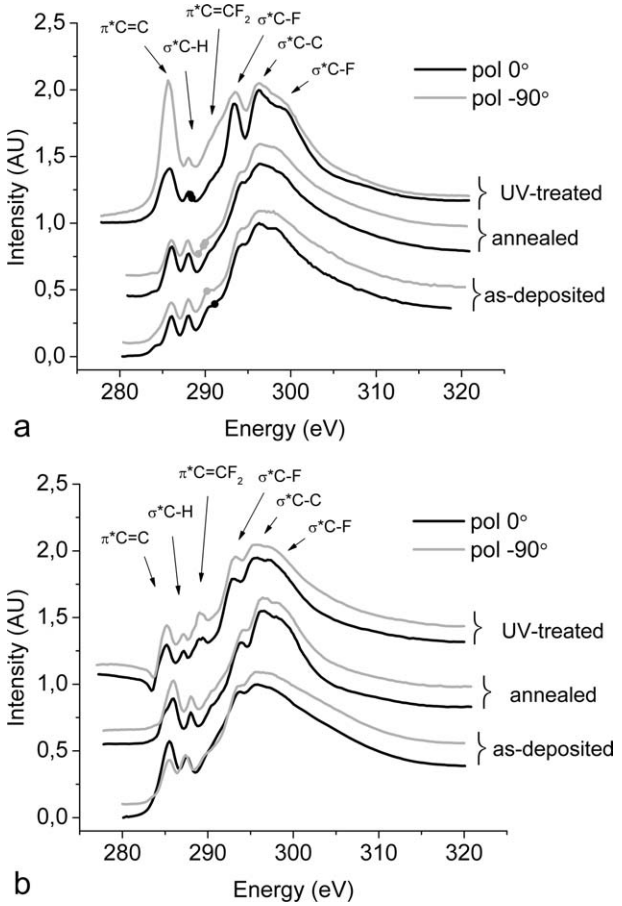

Figure 2 NEXAFS carbon spectra at 0 and −90° polarization for the as-deposited, annealed, and UV-irradiated films (a) before and (b) after deformation.

Therefore, the UV treatment created a chemical composition richer in both C═C and C—C; this was attributed to unsaturated moieties and crosslinking, respectively. This phenomenon was also described in the work of Oshima et al.,[47] where various sorts of double bonded structures were produced in addition to crosslinking sites after the irradiation of PTFE. Moreover, the beam polarization had a major effect on the π* C═C transition at 285 eV. This band was clearly enhanced at the −90° polarization; this indicated that the orientation of the C═C components was essentially along the sample surface plane. In addition, when the Fe 2p signal for a UV-treated specimen was screened, a significant decrease in metallic compounds was measured compared to the as-deposited film [Fig. 3(a)]. The observed decrease in metallic signals suggests that surface reorganization occurred by UV light through the formation of in-plane unsaturations and crosslinks, which shrunk the nanopinholes initially detected in the as-deposited films. This reorganization could be explained by a crystallization process during UV exposure. Indeed, when we focused on the 293- and 295-eV bands (due to C 1s to σ* C—C and σ* C—F transitions) before and after UV treatment, a rather similar intensity in both signals was observed. Compared to the as-deposited specimens however, a higher resolved fine structure was observed for the UV-treated samples; this indicated a less amorphous film containing highly crystalline domains.

After deformation of the specimens, significant variations in intensity were observed for the different functionalities [Fig. 2(b)]. When the spectra of an untreated deformed sample were compared to those of an as-deposited specimen [from Fig. 2(a)], the −90° polarization signal was rather similar. When polarization was shifted to 0° however, the π* C═C transition at 285 eV was more intense than its neighboring 288-eV signal. The latter indicated that during plastic deformation, the cleavage of unsaturated functionalities (C═C) preferentially occurred in-plane and left the majority of the vinyl compounds perpendicular to the surface intact. After UV treatment, the 290-eV transition, assigned to terminal $C{=}CF_2$ moieties,[48] had become more resolved after

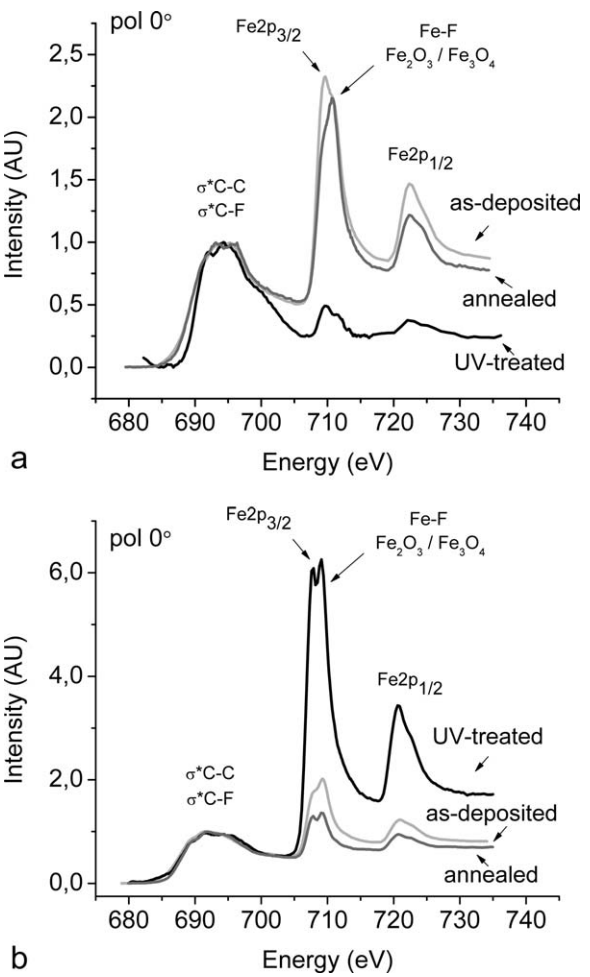

Figure 3 NEXAFS fluorine and iron spectra at 0° polarization for the as-deposited, annealed, and UV-irradiated films (a) before and (b) after deformation.

deformation. The latter could have indicated that deforming the UV treated, more crosslinked film induced chain scission and, in this way, was responsible for the enhanced absorbance by the terminal polymeric groups.

The earlier hypothesis of UV-induced crystallinity could also explain why after plastic deformation, the fine structure in the 290–300-eV band had mainly disappeared [Fig. 2(b)]. Polymeric films with a high crystalline character are known to be less resistant to film rupture during deformation and, in this case, led to a damaged and, again, more amorphous coating. This is confirmed in Figure 3(b), where in contrast to a nontreated deformed specimen, an intense Fe 2p signal was noticed. The signal ratio of the double peak shifted toward the iron oxide shoulder and confirmed the presence of cracks with an oxidized interface. So, whereas before deformation the nanopinholes were partially closed by UV irradiation, deformation significantly reopened these nanoscaled failures because of a loss in the elastic properties.

NEXAFS analyses of the thermally annealed films displayed no significant variation of the surface composition compared to the as-deposited films even after the polarization angle was varied [Fig. 2(a)]. After plastic deformation, similar spectral features were noticed [Fig. 2(b)]. Compared to the deformed UV-treated films, the 290-eV transition (assigned to terminal C=CF_2 moieties) was less resolved; this indicated that polymeric chain scission was a minor phenomenon after thermal annealing. In addition, few differences in the metallic signals were observed after thermal annealing compared to the as-deposited films [Fig. 3(a,b)]. For a flat sample, the Fe $2p_{3/2}$ region displayed a high-energy shoulder (at 709 eV), which was assigned to Fe—F bonds. As thermal annealing was carried out *in vacuo*, no oxidation of the iron was expected to take place. The latter shoulder was, in this way, assigned to the migration of fluorine to the metallic interface and not to the presence of iron oxides. After deformation, both the low- and high-energy shoulders in the Fe $2p_{3/2}$ signal were present; this indicated a partially oxidized iron interface.

ToF–SIMS characterization was performed to verify the effect of the posttreatments on the topmost surface polymeric structure. The spectra displayed a series of signals for the fluoropolymer samples similar to those of PTFE at $m/z = 31$, 81, 131, and 181, which were assigned to C_nF_{2n-1} mass fragments, such as CF, C_2F_3, C_3F_5, and C_4F_7, respectively. These fragments were due to the scission of CF_2 chains, as described by Castner et al.[43] Aligned long chains of polymeric molecules were evidenced through the C_nF_{2n+1} mass fragments, such as $m/z = 69$, 119, 169, and 219 assigned to CF_3, C_2F_5, C_3F_7, and C_4F_9, respectively (end groups). Both sets of mass fragments were visible in the spectra for the differently posttreated fluoropolymers.

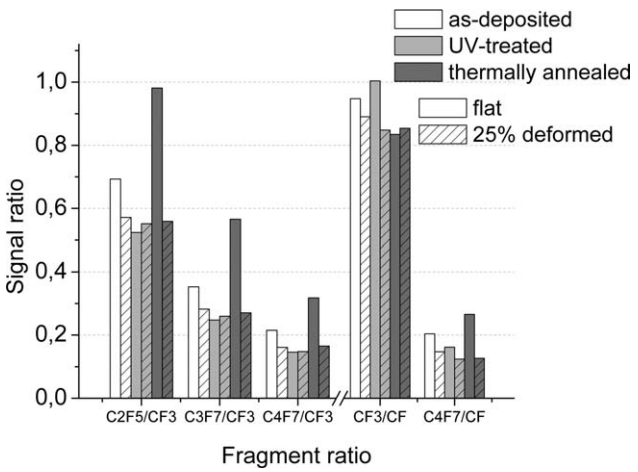

Figure 4 Intensity ratios of the major ToF–SIMS mass fragments as a function of posttreatment.

Figure 4 presents some intensity ratios for the major mass fragments before and after posttreatment and deformation. When we focused on the end-group ratios C_2F_5/CF_3 and C_3F_7/CF_3, significantly longer end groups were present in the nondeformed thermally annealed coatings. Also, an increase in larger polymeric chains was clear for this type of specimen, as observed by the high C_4F_7/CF_3 ratio. We could argue that the increase in the latter ratios could have been due to a drop in CF_3 content; however, the CF_3/C ratios proved to be constant for all specimens. In this way, the ToF–SIMS data tended to confirm the XPS data discussed earlier, where a constant F/C ratio was observed, accompanied by an increase in the CF_2 content. The induction of larger polymeric fragments was probably due to the preferential cleavage of chains on the crosslink sites, where the highest steric strains occurred during heating. Subsequently, these radical linear chain groups could recombine to yield longer chain lengths (and, thus, longer end groups).[49] We could argue that the latter observations during the annealing process could simply be a desorption of less strongly linked polymeric fragments by heat. The applied annealing temperature in this study, however, was much lower than known decomposition temperatures for fluorocarbon films and should not have resulted in mass loss.[36,37]

After deformation, no significant differences in the ratios remained between the annealed and as-deposited specimens. It seemed that the larger fragments rich in CF_2 disappeared, probably because of chain scission induced by the stretching, as observed previously,[23] which affected the longest chains the most.

For UV-treated specimens, only minor variations in the signal ratios were observed. The C_4F_7/CF_3

TABLE II
F/C and O/C Ratios (Calculated from the XPS Survey Data) and C—C, *C*—CF, CF, CF_2, and CF_3 Contents (Obtained from the XPS C1s High-Resolution Scans) from Samples Aged for 2 Weeks

	Deformation	F/C	O/C	% CC/CH	% *C*—CF	% CF	% CF_2	% CF_3
As-deposited	0%	1.60 ± 0.14	0.04 ± 0.01	6 ± 6	20 ± 3	16 ± 2	43 ± 4	15 ± 2
	25%	1.47 ± 0.18	0.08 ± 0.04	16 ± 7	14 ± 3	12 ± 3	44 ± 6	11 ± 3
UV-treated	0%	1.67 ± 0.03	0.06 ± 0.01	7 ± 5	18 ± 3	13 ± 2	48 ± 2	14 ± 3
	25%	1.35 ± 0.13	0.07 ± 0.02	19 ± 7	16 ± 1	18 ± 3	36 ± 3	11 ± 1
Annealed	0%	1.66 ± 0.09	0.04 ± 0.01	2 ± 2	21 ± 4	15 ± 3	11 ± 2	14 ± 1
	25%	1.60 ± 0.01	0.06 ± 0.03	10 ± 4	16 ± 3	14 ± 2	48 ± 3	12 ± 2

All data are presented as a function of treatment and before and after deformation.

ratio decreased slightly, compared to the as-deposited film; this indicated chain scission and crosslinking, which led to shorter end groups. The ToF–SIMS results agreed with the XPS data, where a decrease in the F/C ratio and constant CF_2 content was measured. Plastic deformation had no additional effect on the intensity of the polymeric fragments, as the chains were already shortened.

The CF_3/CF and C_4F_7/CF ratios were also studied, namely, the ratios of two end groups (short and long, respectively) over CF as an omnipresent mass fragment (Fig. 4). Similar conclusions were drawn after we interpreted the latter ratios. After UV treatment, a higher fraction of short end groups (CF_3) was measured, which conformed to the hypothesis of chain scission and crosslinking. In contrast, an enhanced level of long polymeric chain fragments (C_4F_7) was present in the thermally annealed films; this confirmed the phenomenon of film reorganization by heat.

Infrared spectroscopy (ATR–FTIR), which yielded information about the chemical composition of the entire film (maximum of 1-μm depth analysis), displayed no significant variation in the spectral features before and after posttreatment (data not shown), as opposed to the surface phenomena discussed previously, which were detected within the top layers (5–10 nm for XPS and NEXAFS and 1–2 nm for Tof–SIMS) of the 35-nm thin fluorocarbon films.

AFM yielded valuable information about the roughness and morphology of the films before and after the different treatments. R_{RMS} data were calculated from 20 × 20 μm^2 images and amounted for flat specimens to 5.6 ± 0.5 nm (as-deposited), 6.6 ± 0.5 nm (UV-treated), and 6.5 ± 0.5 nm (thermally annealed) and, so, displayed no significant variation. After deformation, R_{RMS} values of 150 ± 80 nm (as-deposited), 210 ± 80 nm (UV-treated), and 140 ± 70 nm (thermally annealed) were obtained. The increase in the AFM roughness coefficient after deformation and the relatively high standard deviations on the mean were directly related to the presence of slip bands induced by the plastic deformation, as previously discussed.[22] Moreover, no significant influence of the posttreatments on the film topography was observed.

Finally, the film thickness was measured by ellipsometry and yielded films around 35 nm (with high standard deviations inherent to the technique). Posttreatments proved to have no significant influence on the coating thickness.

Effect of the posttreatment on the stability of the fluorocarbon films

The fluorocarbon films, both as-deposited and posttreated, were subjected to an aging procedure for 2 weeks in deionized water. The surface composition was thereafter studied.

The XPS survey analyses showed a drop in the fluorine content for all samples, accompanied with an increase in oxygen (Table II). Stability studies on fluorocarbon films showed earlier that incubation in water led to oxidation-induced defluorination processes induced by the penetration of water through the nanodefects present in the films.[24] Here, the loss in fluorine was mainly a drop in CF_2 content, as proved by high-resolution XPS data. For flat specimens, this decrease in CF_2 could be correlated with the observed increase in *C*—CF moieties during aging. After plastic deformation, however, fewer *C*—CF functionalities were measured after aging and, in this way, displayed an opposite trend. The latter was related to the formation of fluorine-poor C—C/C—H functionalities for the deformed aged samples, as measured by XPS (18 ± 7% for as-deposited, 19 ± 7% for UV-treated, and 10 ± 4% for annealed films). For flat aged samples, the number of these C—C/C—H moieties on the surface was always limited (between 3 and 6%).

Although NEXAFS analyses on as-deposited and annealed specimens displayed no difference before and after water aging, valuable information could be extracted from UV-irradiated samples after aging (Fig. 5). The spectra for aged flat samples were identical to those before aging, where the same effect of the beam polarization on the π* C=C transition at 285 eV was observed. The latter indicated that the

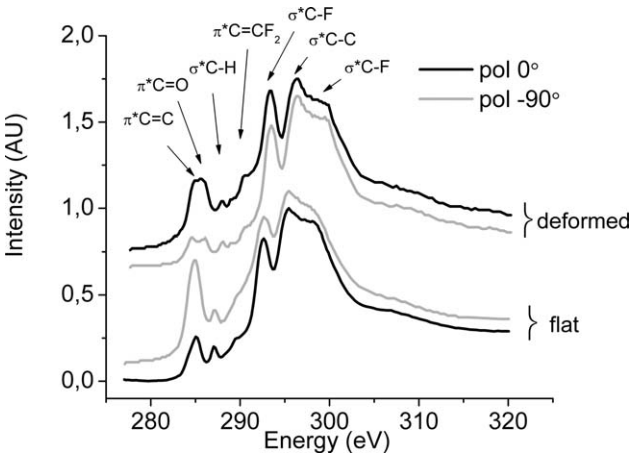

Figure 5 NEXAFS carbon spectra at 0 and −90° polarization of the UV-irradiated films after 2 weeks of aging.

orientation of C=C functionalities essentially remained in the sample surface plane. Moreover, during the aging procedure, water was hampered to penetrate the film by the shrinkage of the nanopinholes induced by UV irradiation [less Fe detected in F—Fe NEXAFS spectra, Fig. 3(a)]. After plastic deformation and aging, however, a new band appeared at 286.5 eV, which was assigned to C 1s to π* C=O transitions.[50] The reason for appearance of the latter band was assumed to be the following. Vinylic $C=CF_2$ terminal groups, which were demonstrated to be present in the UV-treated deformed samples [Fig. 3(b)], were oxidized during aging, which explained in the first case their disappearance in the NEXAFS spectrum for aged samples (Fig. 5). Second, ketone residues are presumably the most important oxidation products of terminal vinyl groups, are known to absorb around 286–287 eV, and in this way, were responsible for this π transition high-energy shoulder. Although before deformation the intensity of the −90° polarized band at 285 eV was higher compared to the 0° polarized spectrum, this phenomenon was now the opposite after deformation. So, unsaturated species, such as C=C and C=O, seemed to be more orientated perpendicular to the surface plane after deformation and aging. Earlier, before the aging process, deformation of the UV-treated samples clearly exhibited that the bands at 285 and 290 eV, assigned to π* C=C and π* $C=CF_2$, respectively, were not influenced by the polarization [Fig. 2(b)]. The latter indicated that after deformation, the unsaturations were less organized in the surface plane compared to the orientation observed before the deformation process [Fig. 2(a)]. These observations led to the assumption that during aging, oxidation of the UV-treated film after the deformation process induced a reorganization of oxidized chain ends. The presence of the C 1s to σ* C—O band, due to the film oxidation during the aging process, was not distinguished as the latter overlapped with the C—C band at the same 292–293-eV energy level. So, additional information about film oxidation could not be provided by NEXAFS.

Figure 6 presents the F—Fe NEXAFS spectra for the aged specimens. For all aged films, the signal ratio of the double peak mainly shifted toward the iron oxide shoulder, which confirmed the presence of an oxidized interface due to aging. Similar to the nonaged samples, the smallest amount of metallic compounds was measured in the case of the UV-treated films; this indicated that the shrunken pinholes did not reopen during aging [Fig. 6(a)]. When the Fe 2p signal was screened after deformation, its intensity remained very low for the UV-treated specimen [Fig. 6(b)]. The size of the pinholes, which had increased during the deformation of the UV-irradiated film, seemed to have decreased during aging. This was probably due to the previously observed swelling of the film caused by the uptake of water during immersion.[24]

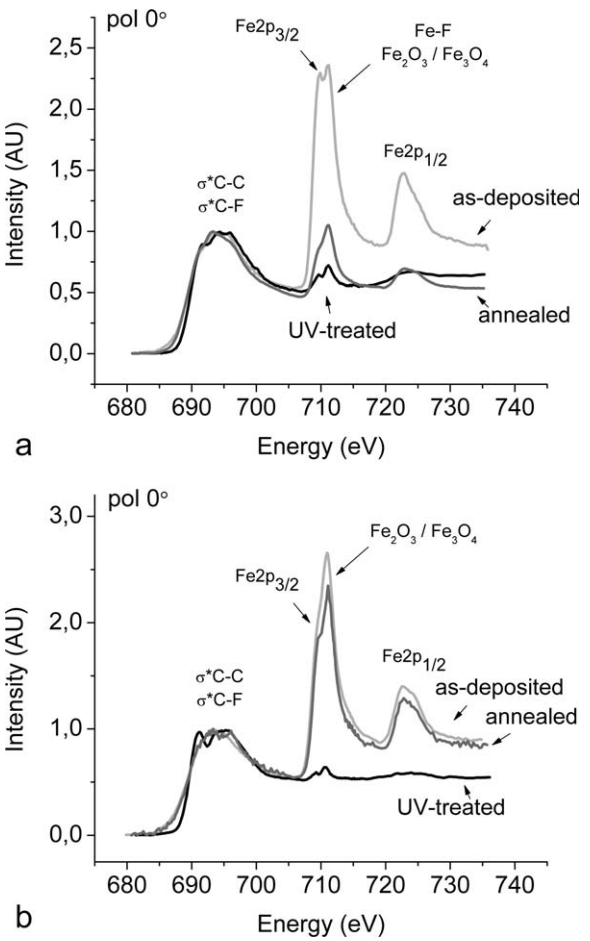

Figure 6 NEXAFS fluorine and iron spectra at 0° polarization for the as-deposited, annealed, and UV-irradiated films after 2 weeks of aging (a) before and (b) after deformation.

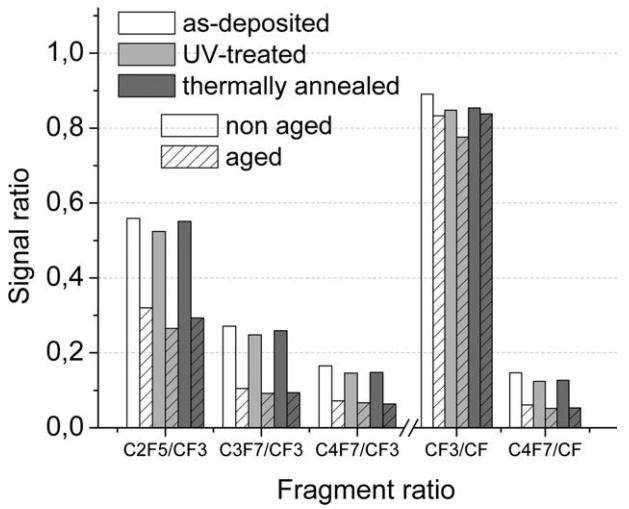

Figure 7 Intensity ratios of the major ToF–SIMS mass fragments for the deformed samples as a function of posttreatment after 2 weeks of aging.

Figure 7 shows the ToF–SIMS intensity ratios for major mass fragments of the deformed samples before and after aging. The quantity of longer end groups and polymeric chains present in the films was clearly lowered after aging; this indicated chain scission and oxidation during incubation in water. No significant differences were observed among the different posttreatments for the deformed and aged samples. Probably, the effect of aging (defluorination and oxidation) became the dominant surface phenomena and, in this way, concealed the effects induced by the posttreatments. Again, oxidized fragments could be hardly differentiated because of the various degrees of oxidation and overlap with the nonoxidized fragments.

CONCLUSIONS

The use of XPS and the highly sensitive techniques NEXAFS and ToF–SIMS provided interesting information about the chemical composition of posttreated fluorocarbon polymers. UV treatment led to a more crosslinked and unsaturated surface with a lower nanopinhole density compared to as-deposited films. These were apparently shrunken by the unsaturations and crosslinking, which clearly occurred along the surface plane according to the polarized NEXAFS analyses. Thermal annealing made the proportion of long chains increase by preferential scission at the crosslink sites and, in this way, reorganized the surface molecular architecture of the coating.

However, the deformation process induced chain scissions with reorganization for both the as-deposited and annealed samples. Whereas before the deformation of UV-treated samples the nanopinholes were partially closed, deformation significantly reopened them because of a loss in elastic properties.

Finally, after the aging tests, the UV treatments proved to have a beneficial effect on the film stability in both the nondeformed and deformed samples. NEXAFS spectra of F—Fe clearly displayed fewer metallic compounds after aging of the UV-irradiated films; this indicated a reclosing of the nanopinholes.

In regard to stent applications, UV irradiation was demonstrated to be the most efficient posttreatment in altering the organization of the polymeric chains in the films. Moreover, this strategy provided a way to decrease the density of nanodefects present in the as-deposited films and significantly enhanced their stability during aging before and after plastic deformation. Optimization of the wavelength used could further these improvements.

The authors thank Bastian Douhard and Nicolas Mine of the Laboratoire Interdisciplinaire de Spectroscopie Electronique (Namur, Belgium) for their help and advice in the ToF–SIMS experiments. The authors also thank Uday Lanke from CLS and Stephen Urquhart from the University of Saskatchewan for their help and guidance in the NEXAFS measurements. The authors also acknowledge the contributions and precious comments provided by Francois Lewis, Penelope Hale, and Cecile Lepelletier.

References

1. Otsuka, Y.; Chronos, N. A. F.; Aptakarian, R. P.; Robinson, K. A. J Invasive Cardiol 2007, 19, 71.
2. Kaba, M.; Essamri, A.; Mas, A.; Schue, F.; George, G. A.; Cardona, F.; Rintoul, L.; Wood, B. J. J Appl Polym Sci 1996, 100, 3579.
3. López, R.; Sanchis, R.; García, D.; Fenollar, O.; Balart, R. J Appl Polym Sci 2009, 111, 2992.
4. O'Keefe, M. J.; Rigsbee, J. M. J Appl Polym Sci 1994, 53, 1631.
5. Walker, M.; Baumgärtner, K.-M.; Ruckh, M.; Kaiser, M.; Schock, H. W.; Räuchle, E. J Appl Polym Sci 1997, 64, 717.
6. Wijesundara, M. B. J.; Zajac, G.; Fuoco, E.; Hanley, L. J Adhes Sci Technol 2001, 15, 599.
7. Jampala, S. N.; Sarmadi, M.; Manolache, S.; Denes, F. S. J Appl Polym Sci 2008, 107, 1686.
8. Grundmeier, G.; Thiemann, P.; Carpentier, J.; Barranco, V. Surf Coat Technol 2003, 174, 996.
9. Gengenbach, T. R.; Vasic, Z. R.; Chatelier, R. C.; Griesser, H. J. J Polym Sci Part A: Polym Chem 1994, 1399, 32.
10. Yanev, V.; Krischok, S.; Opitz, A.; Wurmus, H.; Schaefer, J. A.; Schwesinger, N.; Ahmed, S.-I.-U. Surf Sci 2004, 566–568, 1229.
11. Grundmeier, G.; Reinartz, C.; Rohwerder, M.; Stratmann, M. Electrochim Acta 1998, 165, 43.
12. Joshi, P. P.; Pulikollu, R.; Higgins, S. R.; Hu, X.; Mukhopadhyay, S. M. Appl Surf Sci 2006, 5676, 252.
13. Moffitt, C. E.; Reddy, C. M.; Yu, Q. S.; Wieliczka, D. M.; Yasuda, H. K. Appl Surf Sci 2000, 481, 161.
14. Grundmeier, G.; Stratmann, M. Mater Corros 1998, 150, 49.
15. Mazumder, M. M.; De, S.; Trigwell, S.; Ali, N.; Mazumder, M. K.; Mehta, J. L. J Biomater Sci 2003, 1351, 14.
16. Migliavacca, F.; Petrini, L.; Montanari, V.; Quagliana, I.; Auricchio, F.; Dubini, G., Med Eng Phys 2005, 13, 27.
17. Caicedo, M.; Jacobs, J. J.; Redyy, A.; Hallab, N. J. J Biomed Mater Res A 2008, 905, 86.

18. International Agency for Research on Cancer (IARC). Monographs of the Evaluation of Carcinogenic. Risks to Humans. Vol. 74, Ed. IARC Press: Lyon, France; 1998.
19. Barranco, V.; Carpentier, J.; Grundmeier, G. Electrochim Acta 2004, 1999, 49.
20. Lin, Y.; Yasuda, H. J Appl Polym Sci 1996, 543, 60.
21. U.S. Food and Drug Administration (FDA). Guidance for Industry and FDA Staff; Non-clinical Tests and Recommended Labelling for Intravascular Stents and Associated Delivery Systems; Ed. FDA: Rockville, MD; 2005.
22. Lewis, F.; Horny, P.; Hale, P.; Turgeon, S.; Tatoulian, M.; Mantovani, D. J Phys D: Appl Phys 2008, 41, 045310.
23. Hale, P.; Turgeon, S.; Horny, P.; Lewis, F.; Brack, N.; Van Riessen, G.; Pigram, P.; Mantovani, D. Langmuir 2008, 7897, 24.
24. Touzin, M.; Chevallier, P.; Lewis, F.; Turgeon, S.; Laroche, G.; Mantovani, D. Surf Coat Technol 2008, 4884, 202.
25. Dong, B.; Manolache, S.; Somers, E. B.; Lee Wong, A. C.; Denes, F. S. J Appl Polym Sci 2005, 485, 97.
26. Chevallier, P.; Castonguay, M.; Turgeon, S.; Dubrulle, N.; Mantovani, D.; McBreen, P. H.; Wittmann, J.-C.; Laroche, G. J Phys Chem B 2001, 12490, 105.
27. Griesser, H.; Chatelier, R. J Appl Polym Sci: Appl Polym Symp 1990, 361, 46.
28. Mark, J. E. Physical Properties of Polymers Handbook; AIP: Woodbury, NY, 1996.
29. Dixon, D. A.; Smart, B. E.; Krusic, P. J.; Matsuzawa, N. J Fluor Chem 1995, 209, 72.
30. Haidopoulos, M.; Turgeon, S.; Laroche, G.; Mantovani, D. Plasma Processes Polym 2005, 424, 2.
31. Favia, P. In Plasma Polymer Films; Biederman, H., Ed.; Imperial College Press: London, 2004.
32. Briggs, D. Surf Interface Anal 1989, 209, 14.
33. Polizu, S.; Maugey, M.; Poulin, S.; Poulin, P.; Yahia, L. H. Appl Surf Sci 2006, 6750, 252.
34. Leonard, D.; Bertrand, P.; Shi, M. K.; Sacher, E.; Martini, L. Plasmas Polym 1999, 97, 4.
35. Horcas, I.; Fernández, R.; Gómez-Rodríguez, J. M.; Colchero, J. G.-H., J.; Baro, A. M. Rev Sci Instrum 2007, 78, 013705.
36. Maia Da Costa, E. H.; Baumvol, I. J. R.; Radke, C.; Jacobsohn, L. J.; Zamora, R. R. M.; Freire, F. L. J. J Vac Sci Technol A 2004, 2321, 22.
37. Cruden, B.; Chu, K.; Gleason, K.; Sawin, H. J Electrochem Soc 1999, 4590, 146.
38. Van Krevelen, D. W.; Hoftyzer, P. J. Properties of Polymers; Elsevier Scientific: Amsterdam, 1976.
39. Gnanappa, A. K.; O'Murchu, C.; Slattery, O.; Peters, F.; Aszalos-Kiss, B.; Tofail, S. A. M. Polym Degrad Stab 2008, 2119, 93.
40. Gengenbach, T. R.; Griesser, H. J. Surf Interface Anal 1998, 498, 26.
41. Cheun, H.; Liu, X.; Himpsel, F. J.; Knaapila, M.; Scherf, U.; Torkkeli, M.; Winokur, M. J. Macromol 2008, 6463, 41.
42. Genzer, J.; Sivaniah, E.; Kramer, E. J.; Wang, J.; Körner, H.; Char, K.; Ober, C. K.; DeKoven, B. M.; Bubeck, R. A.; Fischer, D. A.; Sambasivan, S. Langmuir 2000, 1993, 16.
43. Castner, D. G.; Lewis, K. B., Jr.; Fischer, D. A.; Ratner, B. D.; Gland, J. L. Langmuir 1993, 537, 9.
44. Fujimori, A.; Araki, T.; Nakahara, H.; Ito, E.; Hara, M.; Ishii, H.; Ouchi, Y.; Seki, K. Langmuir 2002, 1437, 18.
45. Soriano, L.; Abbate, M.; de Groot, F. M. F.; Alders, D.; Fuggle, J. C.; Hofmann, S.; Petersen, H.; Braun, W. Surf Interface Anal 1993, 21, 20.
46. Krasnikov, S. A.; Vinogradov, A. S.; Preobrajenski, A. B.; Gridneva, L. K.; Molodtsov, S. L.; Laubschat, C.; Szargan, R. Phys Scr 2005, T115, 1074.
47. Oshima, A.; Miura, T.; Asano, S.; Ichizuri, S.; Li, J.; Ikeda, S.; Iida, M.; Matsuura, C.; Tabata, Y.; Katsumura, Y.; Washio, M. Radiat Phys Chem 2001, 39, 62.
48. McLaren, R.; Clark, S. A. C.; Ishii, I.; Hichcook, A. P. Phys Rev A 1987, 1683, 36.
49. Cruden, B.; Chu, K.; Gleason, K.; Sawin, H. J Electrochem Soc 1999, 4597, 146.
50. Jordan-Sweet, J. L.; Kovac, C. A.; Goldberg, M. J.; Morar, J. F. J Chem Phys 1988, 2482, 89.